energies

MDPI

Article

The Nexus Between Heat and Vacuum Pumps: A Novel Hybrid Desalination System

Evgeny V. Solomin [1,*], Konstantin V. Osintsev [1], Andrey S. Martyanov [2] and Nikita A. Pshenisnov [1]

[1] Department of Industrial Thermal Power Engineering, South Ural State University (National Research University), 454080 Chelyabinsk, Russia; osintcevkv@susu.ru (K.V.O.); pshenisnovna@susu.ru (N.A.P.)
[2] Department of Electric Power Generation Stations, Network and Supply-Systems, South Ural State University (National Research University), 454080 Chelyabinsk, Russia; martianovas@susu.ru
* Correspondence: solominev@susu.ru

Abstract

The thermal vacuum distillation of seawater, preheated by a hybrid solar heat pump, is a candidate technology for autonomous and hot-climate sites, but experimental energy and exergy data for it are scarce. The objective of this study is to determine the energy and exergy characteristics of a laboratory vacuum distiller and to describe them with a semi-empirical model whose validity limits are stated explicitly. A 5 L batch distiller was tested at four temperature/pressure regimes (75 °C/0.4 atm, 85 °C/0.6 atm, 90 °C/0.7 atm and 100 °C/1 atm). The model combines empirical correlations for heating and maintenance energies with an evaporation fraction; this is calibrated on the four regimes and restricted to physically admissible conditions. The productivity increased from 125 to 334 g/h, and the specific energy consumption was 3.8–5.7 Wh/g. The vacuum regime had the highest specific energy consumption (5.7 Wh/g against 3.8–4.1 Wh/g at 85–100 °C), so no energy advantage of vacuum operation was demonstrated. The calibrated model reproduced measured productivity and total energy values within 2.7% and 4.5%, respectively; leave-one-out cross-validation gave errors up to 94%, so the predictive capability of the model is limited and the model should be regarded as a descriptive fit of the four measured regimes. The eight model parameters were fitted to twelve measured values, and no independent validation data were available. The effect of pressure cannot be separated from that of temperature, because the two variables increase together (correlation coefficient, 0.99). The exergy efficiency was 1.6–3.2%: 93.8–95.8% of the fuel exergy was destroyed by irreversibilities and 2.6–3.1% was lost with the residual hot water; 41–44% of the exergy destruction occurred in the heating stage. Relative to the minimum work of separation, the second-law efficiency was only 0.014–0.020%. The measured energy inputs exclude the heat pump and the photovoltaic–thermal panel; therefore, the benefit of renewable-energy integration is prospective and was not quantified. Scientific novelty: This study conducts a combined experimental, semi-empirical and exergy assessment of the thermal vacuum distillation of seawater preheated by a hybrid solar-powered heat pump, with explicitly defined model validity limits. Practical contribution: This study presents laboratory-scale reference values of the specific energy consumption and exergy efficiency of the model, and identifies the main loss sources for the design of an industrial prototype. The delivery of distilled water to remote areas by unmanned aerial vehicles is considered only as a prospective application and was not studied.

Keywords: distillation; heat pump; vacuum; seawater; exergy analysis; semi-empirical model

Academic Editor: Chi-Ming Lai

Received: 29 September 2026
Revised: 5 November 2026
Accepted: 6 November 2026
Published: 9 November 2026

Copyright: © 2026 by the authors. Licensee MDPI, Basel, Switzerland. This article is an open access article distributed under the terms and conditions of the Creative Commons Attribution (CC BY) license.

1. Introduction

Freshwater scarcity, caused by population growth and climate change, is a major obstacle to sustainable development [1]. Thermal desalination is energy-intensive. Heat-pump-assisted systems reduce heat demand, but they consume a significant amount of electricity and therefore increase the cost of the distillate [2]. Small-scale desalination driven by renewable energy is of particular interest for hot-climate regions and for autonomous sea navigation. Thermal vacuum distillation is a candidate solution for such applications, since it requires less heat than atmospheric distillation and belongs to a lower class of industrial hazard [3,4]. In the present measurements, however, the vacuum regime did not reduce the specific electrical energy consumption (Section 4). A problem in the research is the lack of experimental energy and exergy data for the vacuum distillation of seawater preheated by a hybrid solar heat pump. These data are needed if we are to assess the feasibility of such a unit and to develop a model that can be used for its design.

Heat-pump-assisted desalination has been studied in several directions, which are reviewed in Section 1.2. Heat pumps have been integrated with humidification–dehumidification (HDH) units to reduce electricity consumption [2] and to improve the efficiency of a two-stage HDH plant [5]. The influence of heat-pump evaporation temperature on the coefficient of performance and on freshwater production has been simulated for a double-effect system [1], a membrane distillation unit with a heat pump has been analyzed to determine its optimal operating characteristics [6], and a solar-powered Stirling-type engine has been investigated for seawater desalination [7]. These studies note the importance of the economic aspect in addition to thermodynamic analyses, and one of the most promising approaches is multi-criteria optimization, which accounts for both the thermodynamic and the economic performance of a desalination plant [8,9]. In addition, numerical methods are used for a preliminary efficiency assessment of evaporation systems operating together with a heat pump [10]. The models of such systems must describe their thermodynamics, and the mass flow rates of both seawater and air affect their performance [11,12].

The paper is organized as follows: Section 1.1 gives the background on heat pumps and exergy analyses, Section 1.2 reviews the literature, and Section 1.3 states the research gap, the aim, the novelty and the practical contribution. Section 2 describes the experimental unit and the semi-empirical model, Section 3 presents the exergy analysis, Section 4 gives the results, including the sensitivity analysis and a discussion of the economic aspects, and Section 5 presents the conclusions.

1.1. Background

A heat pump transforms the energy of a low-potential source into heat that is delivered to the heat carrier through an intermediate refrigerant [13,14]. Its main components are an evaporator, a condenser, a compressor and a control valve [15,16]. Energy analysis gives the balance of incoming and outgoing energy, whereas exergy analysis locates the irreversibilities and the potential for improvement [17–19]. Together, the two approaches are used to assess both the efficiency and the sustainability of thermal systems. The preliminary literature analysis covered heat-exchanger designs for condensers and evaporators, including heat-pipe exchangers [20–32], and solar heat sources for distillation [33–35].

1.2. Literature Review

Published heat-pump-assisted desalination systems can be grouped into humidification–dehumidification (HDH) systems, multi-effect compression systems, membrane distillation and heat-driven concepts; their quantitative indicators are compared in Table 1.

Table 1. Quantitative comparison of heat-pump-assisted desalination systems from the literature and of the present work.

References	System	Method	Main Quantitative Results	Water Cost, USD/m³
[2]	Absorption/thermomechanical heat pump + HDH	Thermoeconomic model	+23.23% freshwater, +47.7% cooling; energy utilization coefficient 6.96	2.051
[5]	Two-stage HDH + heat pump	Aspen Plus simulation	Trends only: higher recovery rate and performance coefficient than single-stage system	–
[1]	Double-effect desalination + compression heat pump	Aspen simulation	Trends only: COP rises and production falls with evaporation temperature	–
[6]	Direct-contact membrane distillation + heat pump (R134a, R22)	Theoretical analysis	COP 1.8–2.1; SEC 330–400 kWh/m³	4–30; 0.5–2 (multi-stage, 2 kW heat pump)
[36]	HDH + heat pump, direct-contact dehumidifier	Thermodynamic model, PSO	89.27 kg/h at GOR 4.17; optimum 150.75 kg/h at GOR 8.12	16
This work	Vacuum distillation of preheated seawater	Experiment (4 regimes) + semi-empirical model	0.125–0.334 kg/h; SEC 3.8–5.7 kWh/kg (≈3800–5700 kWh/m³); exergy efficiency 1.6–3.2%	Not calculated (Section 4.2)

HDH—humidification–dehumidification; COP—coefficient of performance; GOR—gained output ratio; SEC—specific energy consumption. A dash means that no value was given.

In HDH systems, a hybrid thermomechanical heat pump based on a double-effect absorption cycle increased the freshwater production by 23.23% and the cooling output by 47.7% compared with the traditional combination, raised the energy utilization coefficient to 6.96 (+17.89%) and gave a freshwater cost of USD 2.051/m³; the humidifier had the highest energy consumption (8.98 kW, 16.5% of the total) [2]. A two-stage HDH system with a heat pump, modeled in Aspen Plus, showed a higher recovery rate and a higher performance coefficient than the single-stage system at higher seawater inlet temperatures and liquid-to-gas ratios [5]. An open-air, open-water HDH system with a heat pump and a direct-contact dehumidifier, optimized by particle swarm optimization, reached 89.27 kg/h at a gained output ratio of 4.17, and 150.75 kg/h at a ratio of 8.12 without an auxiliary heater, at a freshwater cost of USD 0.016/L [36].

Heat pumps have also been combined with desalination processes other than HDH. A double-effect seawater-desalination system with a compression heat pump was simulated in Aspen: the coefficient of performance increases but the freshwater production decreases with the heat-pump evaporation temperature, and both decrease with the condensation temperature [1]. A high-temperature heat pump was also proposed for the zero-liquid-discharge desalination of supercritical water [37]. Direct-contact membrane distillation integrated with a heat pump (R134a, R22) gave coefficients of performance of 1.8–2.1 and a specific energy consumption of 330–400 kWh/m³ at production costs of USD 4–30/m³ in the closed water cycle, and a parallel multi-stage arrangement with a commercial 2 kW heat pump reduced the cost to USD 0.5–2/m³ [6]. Finally, other heat-driven concepts include a solar-powered Stirling-type engine for seawater desalination [7] and a heat-powered pump that converts heat directly into liquid pressure for reverse osmosis [38].

The cited studies deal mainly with HDH, multi-effect and membrane systems, and most of them are based on simulation. Experimental data for thermal vacuum distillation with preheating by a hybrid solar heat pump, together with exergy indicators, were not found; this is the gap addressed in Section 1.3. For comparison with the electricity-cost estimate of this work, the reported water costs of small-scale solar desalination systems

(capacity below 25 m^3/day [4[39]) are USD 0.2–22/m^3 for small–medium-scale solar plants [40] and USD 15–18/m^3 for autonomous solar membrane distillation units [41]; these values are used as a benchmark in Section 4.2.

1.3. Research Gap, Aim, Novelty and Practical Contribution

Research gap: Heat-pump-assisted desalination has been studied mainly for HDH and membrane systems (Table 1). Experimental data for the thermal vacuum distillation of seawater preheated by a hybrid solar-powered heat pump, exergy assessments based on such data, and models with stated validity limits were not found in the reviewed literature.

Aim, novelty and practical contribution: To close this gap, the aim of this study is to determine, experimentally and with a calibrated semi-empirical model, the productivity, energy consumption and exergy efficiency of a laboratory thermal vacuum distiller at 75–100 °C and 0.4–1 atm, and to define the limits within which the model can be used. The novelty is the combination of experimental data on vacuum distillation of preheated seawater, a calibrated model with explicit physical constraints and validity limits, and a stage-level exergy assessment of the laboratory unit. The reference values of the specific energy consumption and exergy efficiency and the identified loss sources are intended for the design of an industrial prototype; this contribution is prospective, because the heat pump and the photovoltaic subsystem are not included in the measured balances.

2. Materials and Methods (Experimental and Modeling Parts of Study)

2.1. Experimental Part

A hybrid energy system integrating a heat pump and a solar power plant was proposed and developed in an earlier study [13]. The system exploits the complementary advantages of both components while relying exclusively on renewable energy sources. Its distinctive feature is a coil laid on the back side of the solar panel, in which the R407C refrigerant of the heat-pump cycle is additionally heated (Figure 1).

The hybrid unit supplies seawater heated to 75 °C. Heating the feed water is, however, only the first step toward obtaining the distillate; the next step was the development of a distiller. Two options of thermal distillation were considered: distillation at atmospheric pressure with additional heating, or distillation at reduced pressure without additional heating. Based on the basic diagram, a theoretical operating cycle of a vacuum distillation unit was developed (Figure 2) and tested under laboratory conditions.



Figure 1. Hybrid heat pump.



Figure 2. Thermal vacuum distiller.

The experimental data used to calibrate the model are given in Table 2. The measurements were carried out using a thermostat and an RTD10-SCR50-PT1000 temperature sensor (EKF, Moscow, Russia).

Table 2. Experimental data.

	75 °C/0.4 atm	85 °C/0.6 atm	90 °C/0.7 atm	100 °C/1 atm
Amount of water in the evaporator, liters	5	5	5	5
Initial temperature, °C	28.5	29.3	28.9	29.4
Target temperature, °C	75	85	90	100
Average pressure in the evaporator, atm	0.4	0.6	0.7	1
Productivity, g/h	125	217	263	334
The amount of energy spent on heating to the target temperature, W h	310	370	420	630
The amount of energy spent on maintaining the target temperature and creating a vacuum, W h	400	520	580	740

System boundaries: The energy and exergy balances of Sections 2.2–4 refer to the laboratory vacuum distiller only. The electrical energy supplied to the heater (thermostat) during heating and maintenance and to the vacuum pump is counted as the energy input. The hybrid heat pump and the photovoltaic–thermal panel (Figure 1) are not included in the measured energy inputs: they are regarded only as a prospective source of preheated feed water, and no heat-pump electricity or solar heat is included in Table 2 or Table 3. Consequently, the results do not quantify the benefit of renewable-energy integration; this requires a system-level balance, which is outside the scope of the present study.

Table 3. Comparison of the calibrated model with the calibration data.

Parameter	75 °C/0.4 atm	85 °C/0.6 atm	90 °C/0.7 atm	100 °C/1 atm	Max. dev., %
Productivity, g/h (exp.)	125	217	263	334	2.7
Productivity, g/h (model)	126.2	211.1	269.5	333.2	
Total energy, Wh (exp.)	710	890	1000	1370	4.5
Total energy, Wh (model)	686.8	910.5	1044.5	1329.5	
Specific energy, Wh/g (exp.)	5.68	4.1	3.8	4.1	
Specific energy, Wh/g (model)	5.44	4.31	3.88	3.99	
Deviation of productivity, %	+1.0	−2.7	+2.5	−0.2	2.7
Deviation of total energy, %	−3.3	+2.3	+4.5	−3.0	4.5

The process flow of the experimental unit, with the streams and measurement points, is shown in Figure 3.

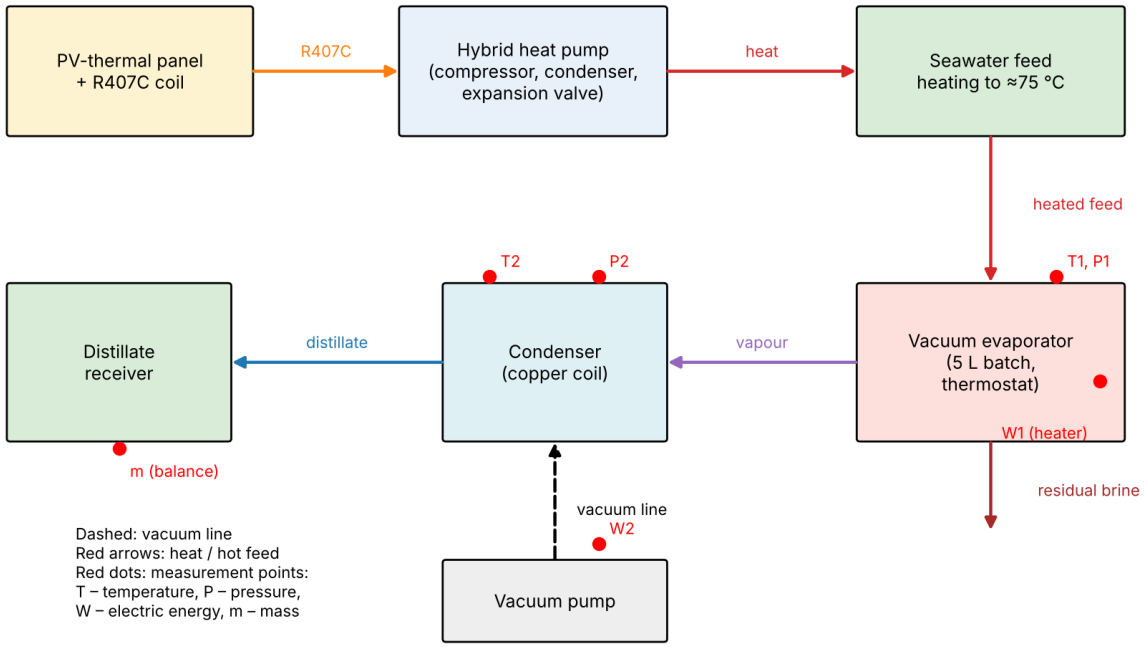


Figure 3. Schematic of the experimental unit and measurement points. T—temperature; P—pressure; W—electric energy; m—distillate mass.

Experimental procedure: A batch of 5 L of seawater was loaded into the evaporator at an initial temperature of 28.5–29.4 °C and heated to the target temperature. The target temperature was then maintained for 1 h at the pressure given in Table 2, and the distillate was collected in the receiver and weighed. The productivity was calculated per hour of steady operation. The unit comprised the evaporator with the heater (thermostat), the vacuum pump, the condenser and the receiver (Figure 3). The temperature was measured by the Pt1000 resistance sensor RTD10-SCR50-PT1000 connected to an TRM500 (OWEN, Moscow, Russia) controller, the pressure by a vacuum gauge and the electric energy by a wattmeter; the vacuum pump had a power of 100 W. The models and accuracies of these instruments, the heater power, the specifications of the condenser and of the balance, the sampling frequency and the number of repeated runs per regime were not recorded; Table 2 gives one value per regime, so the repeatability was not assessed. The seawater composition was not documented: its salinity, conductivity and sampling site were not recorded, and the water activity, $a_w = 0.98$, used in Section 3 is therefore an assumed value.

Measurement uncertainty: The accuracies of the temperature channel (the RTD10-SCR50-PT1000 sensor with the OWEN TRM500 controller), of the vacuum gauge, of the wattmeter and of the balance are not documented, so the measurement uncertainty is not quantified in this study. The standard uncertainties of energy, E, and of productivity, M, are combined into the relative uncertainty of the specific energy consumption as $u(SEC)/SEC = [(u(E)/E)^2 + (u(M)/M)^2]^{1/2}$. The influence of the set-point errors on the model outputs is analyzed in Section 4.1.

To generalize the experimental results within the investigated range, a semi-empirical model of the thermal vacuum distillation unit was developed. The model describes the key physical processes: water heating, evaporation under reduced pressure, and condensation. The empirical parameters of the model are calibrated using the experimental data from Table 2 (Section 2.2). The comparison with these data characterizes the quality of the fit and not the independent predictive accuracy of the model.

2.2. Modeling

The mathematical model is based on the energy balance of the distillation process and consists of three sub-models: (1) heating energy, (2) maintenance energy, and (3) evaporation productivity. The model is a semi-empirical regression: the heating factor has two empirical parameters, the maintenance energy has three, and the evaporation fraction has three; all of them are fitted to only four experimental regimes (Table 2). In total, 12 measured values (the heating energy, the maintenance energy and the productivity in four regimes) are described by 8 parameters, i.e., 4 degrees of freedom (2, 1 and 1 in the heating, maintenance and evaporation sub-models, respectively), so the statistical power of the fit is low.

Heating energy: The energy required to heat the water mass, m_w, from the initial temperature, T_{init}, to the target temperature, T, is calculated as follows [Wh]:

$$Q_{heat} = m_w \cdot c_w \cdot (T - T_{init}) \cdot \eta_{heat}(T)/3.6, \quad (1)$$

where m_w = 5 kg is the water mass, c_w = 4.186 kJ/(kg·K) is the specific heat, and $\eta_{heat}(T) = a_1 \cdot T + b_1$ is the heating factor, i.e., the ratio of the electrical energy consumed to the sensible heat of the water ($\eta_{heat} > 1$ represents heat losses), fitted by unweighted least squares to $\eta_i = Q_{exp,i}/[m_w c_w (T_i - T_{init})/3.6]$ (a_1 = 0.01449, b_1 = −0.0160). The initial temperature was taken as the mean measured value, T_{init} = 29 °C (28.5–29.4 °C), both in the fit and in the calculations. For electric heating, $\eta_{heat} \geq 1$ is required by the first law of thermodynamics; the fitted correlation gives η_{heat} = 1 at 70.1 °C and is therefore physically admissible only for T ≥ 70.1 °C. It is used here only for T ≥ 75 °C, where η_{heat} = 1.07–1.43. The heating sub-model deviates from the measured heating energy by −7.6%, +7.0%, +8.8% and −6.1% in the four regimes, because the measured factor is not linear in T; these errors are partly compensated for by the maintenance sub-model in the total energy.

Maintenance energy: The energy consumed to maintain the target temperature and create vacuum during one hour of operation is modeled as follows [Wh]:

$$Q_{maint} = \alpha \cdot (T - T_{amb}) + \beta/P + \gamma, \quad (2)$$

where T_{amb} = 30 °C is the ambient temperature, P is the absolute pressure in the evaporator (atm), and α = 18.84, β = 89.01, γ = −669.85 are the empirical coefficients obtained by least-squares fitting to the experimental data. The coefficients were obtained by least-squares fitting of the measured maintenance energy (four points, three parameters, one degree of freedom). The correlation gives $Q_{maint} \leq 0$ below about 61 °C at 1 atm and below 50 °C at 0.3 atm, which is physically inadmissible; it is therefore used only inside the admissible domain defined below.

Saturation pressure: The saturation pressure of water vapor as a function of temperature is described by the Antoine equation [Pa]:

$$\log_{10}(p_s) = A - B/(C + T), \quad (3)$$

with Antoine constants A = 10.196, B = 1730.63, and C = 233.426 for water in the temperature range of interest. The Antoine and Watson correlations are taken from [42].

Latent heat of vaporization: The latent heat r(T) decreases with temperature and is approximated by the Watson correlation [kJ/kg]:

$$r(T) = r_{100} \cdot [(T_{crit} - T)/(T_{crit} - 100)]^n, \quad (4)$$

where r_{100} = 2257 kJ/kg is the latent heat at 100 °C, T_{crit} = 374 °C is the critical temperature of water, and n = 0.38 is the empirical exponent.

Evaporation productivity: The distillate productivity is determined by the fraction of maintenance energy directed to evaporation [g/h]:

$$M = f_{evap}(T, P) \cdot Q_{maint} \cdot 3.6/r(T) \cdot 1000, \quad (5)$$

where $f_{evap}(T, P) = c_1 \cdot T + c_2 \cdot P + c_3$ is the evaporation fraction (c_1 = 0.01912, c_2 = −0.6652, c_3 = −0.9637), representing the share of thermal energy converted to vapor. This fraction accounts for heat losses to the environment and the energy consumed by the vacuum pump. The coefficients c_1–c_3 were fitted by least squares to $f_i = M_{exp,i}\, r(T_i)/(3.6 \cdot 10^3\, Q_{maint,exp,i})$, which equals 0.203, 0.267, 0.288 and 0.283 for the four regimes (three parameters, four points). The function f_{evap} is linear and is non-negative only if $T \geq (0.9637 + 0.6652P)/0.01912$, i.e., above 60.8 °C at 0.3 atm and above 85.2 °C at 1 atm; below this line, the model gives a negative productivity, which is physically inadmissible. Within the calibrated corridor, f_{evap} = 0.20–0.29: only 20–29% of the maintenance energy is converted into the latent heat of the distillate.

Specific energy consumption: The overall energy efficiency of the distillation process is characterized by the specific energy per gram of distillate [Wh/g]:

$$q_{spec} = (Q_{heat} + Q_{maint})/M, \quad (6)$$

Admissible domain and validity limits: The model is applied only where (i) $\eta_{heat} \geq 1$, i.e., T ≥ 70.1 °C; (ii) $Q_{maint} > 0$; (iii) $f_{evap} > 0$; and (iv) the pressure is not below the saturation pressure of the liquid at the set temperature, $P \geq P_s(T)$, because otherwise the liquid at this temperature cannot exist and flashes to the saturation temperature of the pressure. On a grid of 50–100 °C and 0.3–1.0 atm, 75% of the points violate at least one of these constraints (46% have $f_{evap} < 0$, 15% have $Q_{maint} < 0$, 40% have $\eta_{heat} < 1$ and 26% lie below the saturation line). The experimental regimes lie on the saturation line: the ratios $P/P_s(T)$ are 1.05, 1.05, 1.01 and 1.00. The model is therefore used for 75 °C ≤ T ≤ 100 °C and $P_s(T) \leq P \leq 1$ atm, and the results outside the corridor $P \leq 1.06P_s(T)$ are extrapolations. Because pressure rises with temperature along the saturation line in all four regimes, the separate effects of T and P cannot be identified from these data. The correlation coefficient between T and P over the four regimes is 0.993 (between T and 1/P, −0.982). For the evaporation fraction, the coefficient c_2 = −0.665 has a standard error of 0.114 with one degree of freedom, so its 95% confidence interval (−2.11 to 0.78) includes zero and the sign of c_2 is not statistically established; the same applies to the term β/P of Equation (2). If c_2 is set to zero (c_1 and c_3 refitted), the maximum deviation of the productivity increases from 2.7% to 8.4%, but this improvement of the fit cannot be attributed to pressure, because T and P are collinear. Experiments at constant temperature and different pressures are required to separate the two effects.

The calibrated model was compared with the four calibration regimes (Table 3). The maximum deviation is 2.7% for productivity (85 °C/0.6 atm) and 4.5% for total energy (90 °C/0.7 atm). This comparison shows how well the correlations fit the data used to determine their parameters; it is not an independent validation, because the model has eight empirical parameters in three sub-models and was fitted to only four regimes.

To estimate the predictive ability, leave-one-out cross-validation was applied: each regime was removed in turn, the parameters were refitted to the remaining three regimes, and the removed regime was predicted (Table 4). For the interior regimes (85 and 90 °C) the errors are 5.9–6.0% in productivity and 2.1–6.2% in total energy, but for the boundary regimes, 75 °C/0.4 atm and 100 °C/1 atm, they reach 94% and 21% in productivity and 30% and 13% in total energy, respectively. Thus, the predictive capability of the model is limited. The only interpolation test available is based on the two interior regimes (errors of about 6% in productivity); two points are too few for a meaningful estimate of the predictive error, so this value must not be regarded as a validation. The model cannot be used for extrapolation.

Table 4. Leave-one-out cross-validation (each regime is predicted by the model fitted to the other three).

	75 °C/0.4 atm	**85 °C/0.6 atm**	**90 °C/0.7 atm**	**100 °C/1 atm**
Productivity (predicted), g/h	242.6	204.3	278.8	403.1
Deviation from experiment, %	+94.0	−5.9	+6.0	+20.7
Total energy (predicted), Wh	921.9	908.5	1062.5	1186.5
Deviation from experiment, %	+29.8	+2.1	+6.2	−13.4

An independent validation requires additional experiments at intermediate regimes, for example at 80 °C and 95 °C. In the present study, such runs were not performed, and the claims about the predictive ability of the model are limited accordingly.

A numerical experiment was conducted to investigate the performance of the thermal vacuum distillation unit over a wide range of operating conditions: temperatures from 75 °C to 100 °C and pressures from the saturation pressure $P_s(T)$ to 1.0 atm (physically admissible domain). The model equations were solved for each combination of temperature and pressure, yielding productivity, energy consumption, and specific energy consumption. The red circles in the figures denote the experimental data points from Table 3. The solid lines in Figures 4 and 5 show the calibrated corridor $P \leq 1.06P_s(T)$; the dashed lines are extrapolations inside the admissible domain.

Figure 4 shows the distillate productivity as a function of temperature for seven pressure levels (0.4–1.0 atm); each curve ends at the saturation temperature of its pressure. Productivity increases monotonically with temperature due to the growing driving force for evaporation. At a given temperature, the fitted model gives a higher productivity at lower pressure; this follows from the signs of the fitted coefficients c_2 and β, which the data do not establish (Section 2.2), and is not an experimental result. The increase with temperature is due to the growth of the evaporation fraction from 0.20 to 0.28 and of the maintenance energy, partly offset by the decrease in the latent heat from 2333 to 2257 kJ/kg. In the model, the higher productivity at a lower pressure arises because the fitted evaporation fraction decreases with pressure ($c_2 < 0$), which the data do not establish (Section 2.2); at the same time, the vacuum term of the maintenance energy increases (222 Wh at 0.4 atm against 89 Wh at 1 atm). The pressure dependence is an extrapolation of the fitted correlations, since $P \approx P_s(T)$ in all four regimes.

Figure 5 presents the total energy consumption (heating + maintenance) as a function of temperature and pressure. Energy consumption rises with temperature due to increased heat losses and greater energy required for heating. The effect of pressure is less pronounced: lower pressures slightly increase the maintenance energy through the vacuum term, β/P, but the difference diminishes at higher temperatures. In the calibrated regimes, only 20–29% of the maintenance energy is converted into the latent heat of the distillate; the remaining 71–80% is lost to the environment and consumed by the vacuum pump.

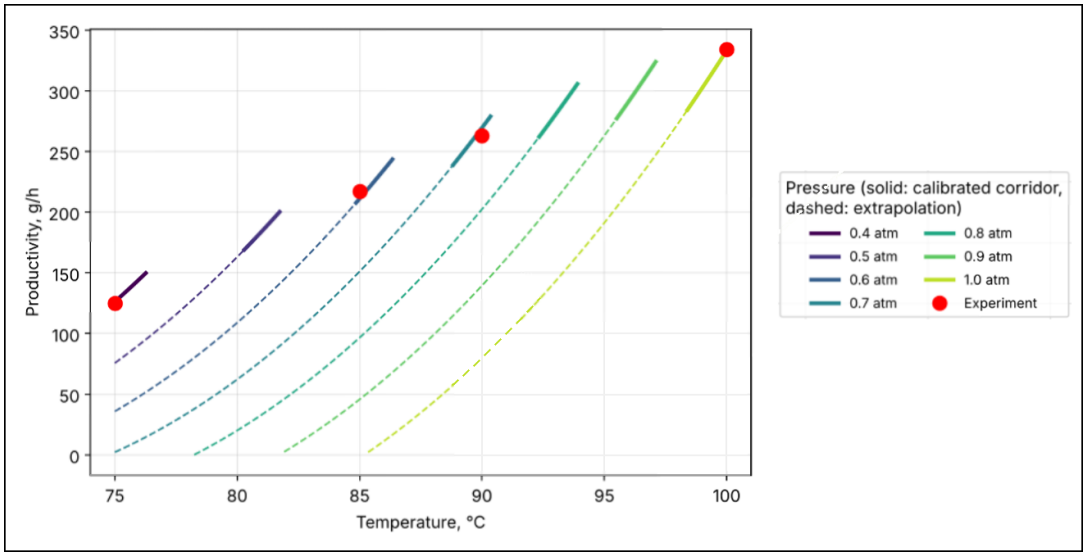


Figure 4. Model productivity vs. temperature at different pressures (red circles: experimental data). Solid lines—calibrated corridor; dashed lines—extrapolation inside the admissible domain.

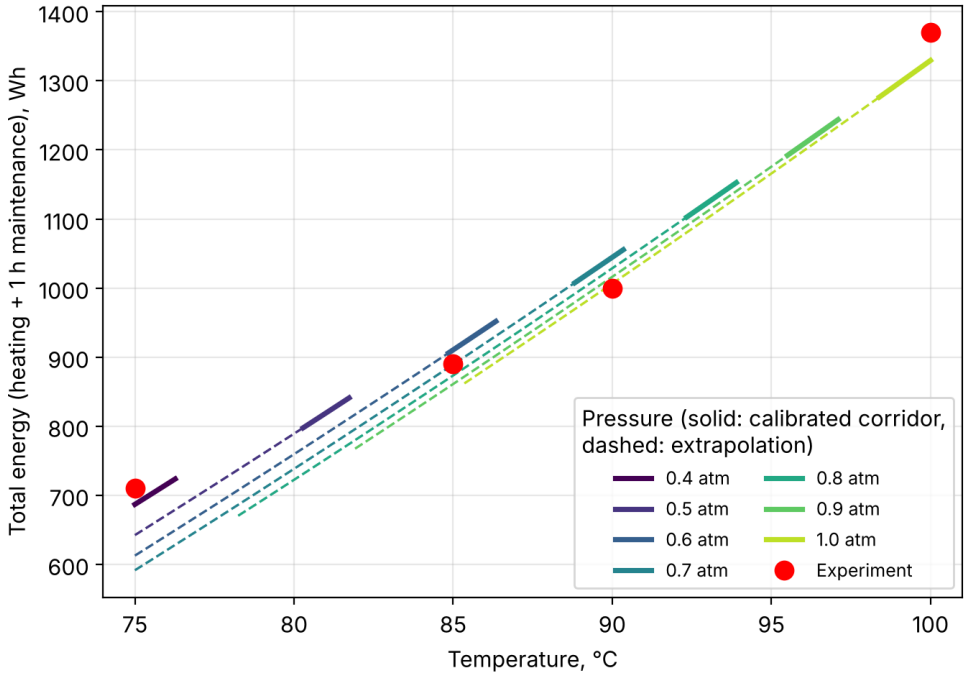
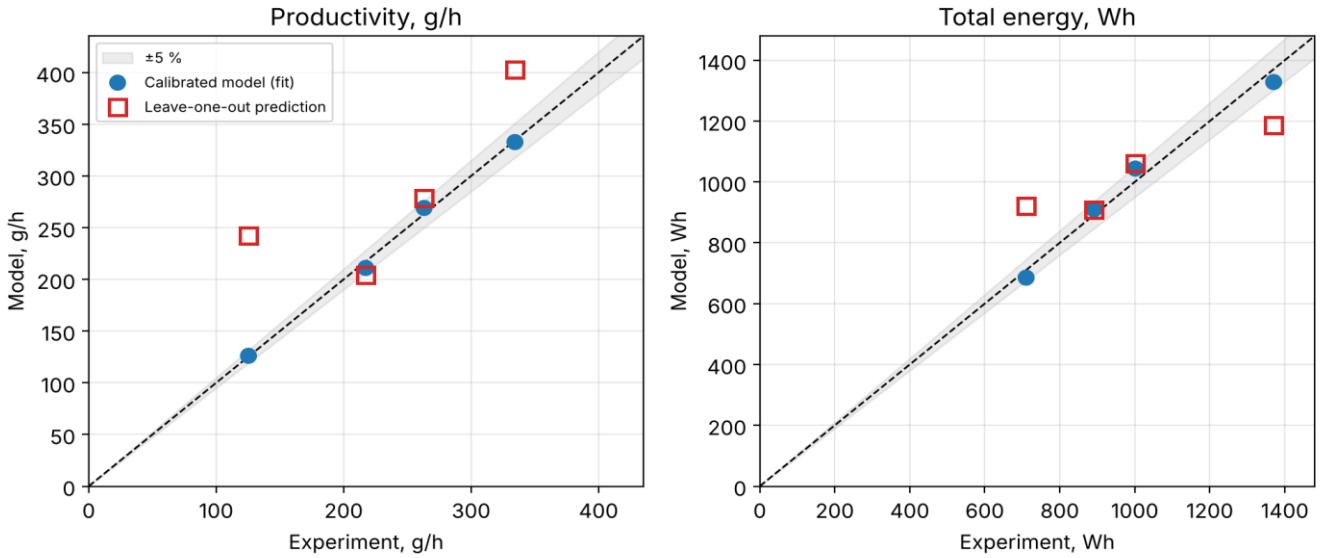


Figure 5. Total energy consumption vs. temperature at different pressures. Red circles—experimental data; solid lines—calibrated corridor; dashed lines—extrapolation inside the admissible domain.

Figure 6 provides a direct comparison between model predictions and experimental measurements. Panel (a) compares productivity values: all calibrated points lie close to the diagonal, with a maximum deviation of 2.7%. Panel (b) compares total energy consumption: the agreement is within 4.5%. The scatter around the diagonal cannot be attributed to measurement uncertainty until the instrument uncertainties are specified; it may also reflect model simplifications (e.g., constant ambient temperature, neglect of salt concentration effects). The open squares show the leave-one-out predictions (Table 4), which deviate strongly from the diagonal for the boundary regimes.



(**a**) (**b**)

Figure 6. Model vs. experiment: left panel (**a**)—productivity; right panel (**b**)—total energy consumption. Dashed line—ideal agreement; open squares—leave-one-out predictions.

3. Exergy Analysis

The required power of the pump:

$$W_{\text{pump}} = \frac{\dot{m}_{\text{fw}}\,\Delta P}{\rho\,\eta_{\text{pump}}} \tag{7}$$

where ρ is the feed water flow density and η_{pump} is the isentropic efficiency of the pump.

The specific energy consumption is

$$\text{SEC} = \frac{W_{\text{pump}}}{\dot{V}_d} \tag{8}$$

The net power consumed by the system is

$$W_{\text{net}} = W_{\text{pump}} + \sum_{i=1}^{n} W_i \tag{9}$$

where $W_1, W_2, W_3,$ and W_4 are the power consumption of pumps 1–4, respectively.

The pump equations above refer to a prospective full-scale configuration with pumps 1–4. In the present study, the net electrical input of the laboratory unit is $Q_{heat} + Q_{maint}$ (Section 2.2, including the vacuum pump), and the specific energy consumption is defined as SEC = $(Q_{heat} + Q_{maint})/M$ in Wh/g; the pump power was not added separately.

Based on the first and second laws of thermodynamics, the steady-state exergy balance is

$$\dot{E}_D = \sum \dot{E}_{\text{in}} - \sum \dot{E}_{\text{out}} \tag{10}$$

where the subscripts "in" and "out" represent the specific exergy at the input and output relative to the control volume, and $\dot{E}_D$ is the destruction of exergy due to the irreversibility of the system. The outgoing exergy ΣE_{out} includes both the product stream and the stream rejected without use (the exergy loss E_L, here the residual hot water), so that, in the notation of Equation (14), $E_F = E_P + E_D + E_L$: exergy destruction, E_D, is generated inside the

control volume by irreversibilities, whereas exergy loss, E_L, is carried out of the control volume by a stream that is not used.

The specific exergy is

$$e = e_{ph} + e_{ch} \quad (11)$$

where e_{ph} and e_{ch} are the physical and chemical exergy, respectively.

The physical exergy is

$$e_{ph} = (h - h_0) - T_0\,(s - s_0) \quad (12)$$

The chemical exergy is

$$e_{ch} = \sum_i x_i\; e^0_{ch,i} + R\,T_0 \sum_i x_i \ln x_i \quad (13)$$

The exergy balance of each component (fuel–product–destruction–loss) is

$$\dot{E}_{F,k} = \dot{E}_{P,k} + \dot{E}_{D,k} + \dot{E}_{L,k} \quad (14)$$

The overall exergy efficiency is

$$\eta_{ex} = \frac{\sum \dot{E}_P}{\sum \dot{E}_F} \quad (15)$$

The basis of the exergy calculation: The reference (dead) state is T_0 = 30 °C (303.15 K) and P_0 = 1 atm, which corresponds to the ambient temperature used in the model. The fuel exergy, E_F, is the total electrical energy supplied to the distiller during the heating stage and one hour of maintenance ($W_{heat} + W_{maint}$), with electricity being pure exergy. The product exergy, E_P, is the exergy of the distillate produced during this hour, $e_{vap} = (h - h_0) - T_0(s - s_0)$, evaluated for saturated vapor at the set temperature relative to liquid water at T_0 with a constant specific heat of 4.186 kJ/(kg·K) and the Watson latent heat r(T); it equals 314.3, 372.4, 400.0 and 452.8 kJ/kg for the four regimes. The thermal exergy of the heated residual water, $E_L = m_w c_w[(T - T_0) - T_0 \ln(T/T_0)]$, minus the same quantity at T_{init}, is rejected at the end of the cycle and is treated as an exergy loss (64–147 kJ). The chemical exergy of seawater, $e_{ch} = RT_0 \ln(a_w)/M_w = -2.8$ kJ/kg at a_w = 0.98, is below 1% of e_{vap} and was neglected. For the stage-level balance, the distiller is divided into the heating stage, $D_{heat} = W_{heat} - E_L$, and the evaporation–condensation–vacuum stage, $D_{dist} = W_{maint} - E_P$, so that $E_F = E_P + E_L + D_{heat} + D_{dist}$. The exergy destruction $D = D_{heat} + D_{dist}$ is thus the exergy consumed by irreversibilities inside the distiller, the exergy loss, E_L, is the exergy of the stream leaving the distiller unused, and $1 - \eta_{ex} = (D + E_L)/E_F$; the three terms are reported separately in Section 4.

Second-law efficiency based on the minimum work of separation: The exergy efficiency E_P/E_F defined above credits the thermal exergy of the vapor and is specific to thermal distillation; it differs from the basis commonly used for desalination, the minimum work of separation. For comparison with the literature, the second-law efficiency is therefore also calculated as $\eta_{II} = M \cdot w_{min}/E_F$, where M is the mass of distillate produced during the hour of maintenance, E_F is the fuel exergy defined above, and $w_{min} = -R \cdot T_0 \cdot \ln(a_w)/M_w$ is the minimum work of separating pure water from seawater of water activity, a_w. At a_w = 0.98 and T_0 = 303.15 K, w_{min} = 2.83 kJ/kg (0.785 kWh/m^3). The value of a_w is assumed (Section 2.1), and the zero-recovery limit is used, which slightly underestimates w_{min} at the recovery of 2.5–6.7% of the batch reached in one hour.

4. Results of the Exergy Analysis

The exergy analysis was performed based on the formulas presented in Section 3, using the experimental data from Table 2 and the calibrated mathematical model from

Section 2.2. The analysis covers four experimental regimes and extends to a wider range of operating conditions (75–100 °C, saturation pressure to 1.0 atm) through numerical modeling. The exergy balance was constructed using the first and second laws of thermodynamics, with the physical exergy calculated as $ex_{ph} = (h - h_0) - T_0(s - s_0)$ and the chemical exergy of seawater as $ex_{chem} = (R \cdot T_0/M_w) \cdot \ln(a_w)$, where $a_w = 0.98$. The exergy of fuel equals the total electrical energy input, and the exergy of product equals the exergy of the distillate vapor. The results for the four experimental regimes are summarized in Table 5.

Table 5. Exergy analysis results for the experimental regimes.

Parameter	75 °C/0.4 atm	85 °C/0.6 atm	90 °C/0.7 atm	100 °C/1 atm
Productivity, g/h	126.2	211.1	269.5	333.2
Total energy, Wh	686.8	910.5	1044.5	1329.5
Specific energy, Wh/g	5.443	4.313	3.875	3.990
Specific exergy of vapor, kJ/kg	314.3	372.4	400.0	452.8
Exergy destruction and loss, kJ	2432.9	3199.2	3652.5	4635.3
Exergy efficiency, %	1.60	2.40	2.87	3.15
Second-law efficiency (minimum-work basis), %	0.0144	0.0182	0.0203	0.0197

Figure 7 presents the exergy analysis results for the four experimental regimes. The exergy efficiency (Figure 7a) increases monotonically with temperature, rising from 1.60% at 75 °C/0.4 atm to 3.15% at 100 °C/1 atm. Despite this improvement, the exergy efficiency remains below 3.2%, i.e., 96.9–98.4% of the fuel exergy is not converted into product exergy. This share consists of two different terms (Table 6): the exergy loss E_L with the residual hot water (2.6–3.1% of E_F) and the exergy destruction by irreversibilities, $D_{heat} + D_{dist}$ (93.8–95.8% of E_F). Table 6 shows the stage-level distribution: the heating stage accounts for 41–44% of the exergy destruction $D_{heat} + D_{dist}$ (the loss E_L is not included) and the evaporation–condensation–vacuum stage for 56–59%. A further split among the evaporator, the condenser, the vacuum pump and the heat losses to the environment requires separate metering of these components and is not possible with the present data. The likely sources are the finite temperature difference in heat transfer, the heat losses to the environment and the work of the vacuum pump.

Table 6. Stage-level exergy balance of the laboratory distiller (calibrated model, one hour of maintenance). The exergy loss, E_L, and the exergy destruction, $D = D_{heat} + D_{dist}$, are shown separately; $E_F = E_P + E_L + D$ (rounding differences do not exceed 0.01 percentage points).

Parameter	75 °C/0.4 atm	85 °C/0.6 atm	90 °C/0.7 atm	100 °C/1 atm
Fuel exergy $E_F = W_{heat} + W_{maint}$, kJ	2473	3278	3760	4786
Heating stage W_{heat}, kJ	1031	1425	1645	2129
Maintenance stage W_{maint}, kJ	1442	1853	2116	2657
Product exergy E_P, kJ	39.7	78.6	107.8	150.9
Loss E_L (residual hot water), kJ	63.6	93.3	109.9	146.9
Destruction in heating stage D_{heat}, kJ	967	1332	1535	1983
Destruction in evaporation–condensation–vacuum stage D_{dist}, kJ	1402	1774	2008	2506
Total destruction $D = D_{heat} + D_{dist}$, kJ	2369	3106	3543	4489
Share of D_{heat} in $D_{heat} + D_{dist}$, %	40.8	42.9	43.3	44.2

Exergy efficiency E_P/E_F, %	1.60	2.40	2.87	3.15
Share of loss E_L in E_F, %	2.57	2.85	2.92	3.07
Share of destruction D in E_F, %	95.82	94.76	94.21	93.78
$(D + E_L)/E_F = 100 - \eta_{ex}$, %	98.40	97.60	97.13	96.85

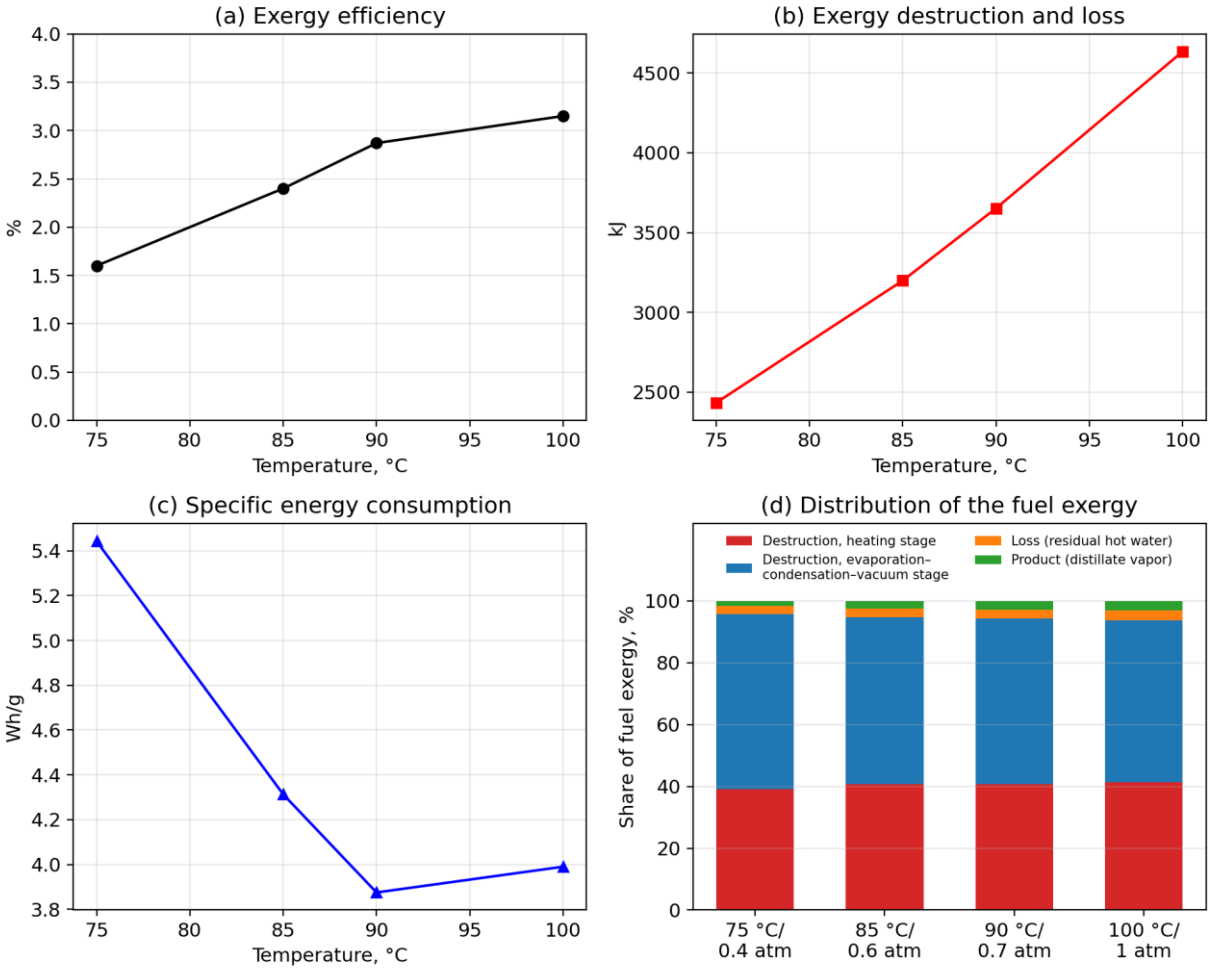


Figure 7. Exergy analysis results: (**a**) exergy efficiency, (**b**) exergy destruction and loss, (**c**) specific energy consumption, (**d**) distribution of the fuel exergy among the product, the loss and the destruction in the two stages.

The sum of the exergy destruction and loss (Figure 7b, Table 5) increases from 2433 kJ at 75 °C to 4635 kJ at 100 °C, following the growth of the fuel exergy from 2473 to 4786 kJ; the exergy loss with the residual hot water accounts for only 64–147 kJ of this sum, and the rest is exergy destruction. The specific energy consumption (Figure 7c) exhibits a minimum of 3.875 Wh/g at 90 °C/0.7 atm, which is the lowest value among the four regimes; however, it is only 3% lower than at 100 °C/1 atm (3.990 Wh/g), i.e., less than the model deviation of 4.5%, so the regimes between 90 and 100 °C cannot be ranked reliably. Figure 7d shows how the fuel exergy is distributed: the product exergy accounts for 1.6–3.2%, the loss with the residual hot water for 2.6–3.1%, and the destruction in the two stages for 93.8–95.8% of the fuel exergy.

On the minimum-work basis, the second-law efficiency is 0.014%, 0.018%, 0.020% and 0.020% for the four regimes (Table 5), i.e., 110–160 times lower than the exergy efficiency based on the vapor exergy (1.6–3.2%). The measured specific energy consumption (3800–5700 kWh/m^3) exceeds the minimum work of separation (0.785 kWh/m^3) by a factor of about 4800–7200. The values of 1.6–3.2% should therefore be compared with the literature

only for processes evaluated on the same vapor-exergy basis; for a comparison with desalination processes in general, the minimum-work basis should be used.

Effect of vacuum on the energy consumption: The measured data do not show an energy advantage of vacuum operation. The specific energy consumption of the vacuum regime 75 °C/0.4 atm (5.68 Wh/g) is the highest of the four regimes, and its consumption for maintenance and vacuum alone (3.2 Wh/g) is higher than at 85, 90 and 100 °C (2.4, 2.2 and 2.2 Wh/g). Per gram of distillate, both the heating energy (2.5 against 1.9 Wh/g) and the maintenance energy (3.2 against 2.2 Wh/g) are higher at 75 °C/0.4 atm than at 100 °C/1 atm. Any advantage of vacuum operation would therefore have to come from the lower temperature of the heat source, which allows the use of low-grade or solar heat; the heat pump and the solar subsystem are not part of the measured balances, so this advantage was not quantified.

The contour map in Figure 8 extends the analysis to the physically admissible domain (75–100 °C, $P_s(T) \le P \le 1$ atm, productivity above 50 g/h). The specific energy consumption has its minimum of about 3.77 Wh/g at 93 °C/0.78 atm on the saturation line, only 3% below the value measured at 90 °C/0.7 atm and within the model deviation; it increases steeply with pressure above the saturation line, because the evaporation fraction decreases. The region below the saturation line (hatched) is physically inadmissible: for example, the saturation temperature is 69.5 °C at 0.3 atm and 76.3 °C at 0.4 atm. Outside the corridor, $P \le 1.06P_s(T)$; the map is an extrapolation and should be treated as qualitative.

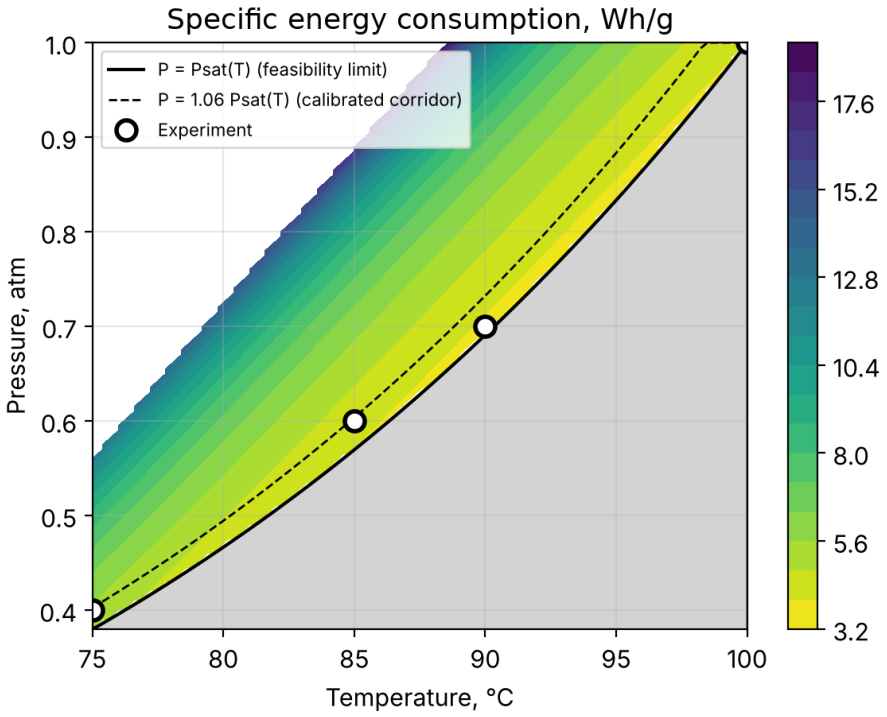


Figure 8. Contour map of the specific energy consumption over the physically admissible domain (solid line, $P = P_s(T)$; dashed line, $P = 1.06P_s(T)$; hatched area—inadmissible region; white circles—experimental regimes).

4.1. Sensitivity and Uncertainty Analysis

The sensitivity of the model outputs to set-point errors is given in Table 7 and is restricted to the admissible domain (75 °C ≤ T ≤ 100 °C, $P_s(T) \le P \le 1$ atm). Because all four regimes lie on the saturation line, the temperature error is applied with the pressure following the saturation line (constant ratio $P/P_s(T)$), so that the perturbed points remain inside the calibrated corridor; the perturbations that would leave the domain (73 °C for the

75 °C regime and 102 °C for the 100 °C regime) are not evaluated (n/a). A temperature error of ±2 °C changes the productivity by 1.8–13.0%, the total energy by 4.5–5.9% and the specific energy consumption by 0.5–6.3%; the sensitivity is the highest at 75 °C. The effect of the pressure alone cannot be studied inside the calibrated corridor, whose width is only about 6% of P_s. An increase in the pressure by 0.05 atm at constant temperature is therefore an extrapolation inside the admissible domain (P/P_s = 1.09–1.19); it is given for qualitative information only, for the three regimes where P + 0.05 atm ≤ 1 atm, and is not applicable to 100 °C/1 atm. It reduces the productivity by 13–22% and increases the specific energy consumption by 14–23%, but these rows depend on the coefficients c_2 and β, which the data do not identify (Section 2.2), and are conditional on the model form. The accuracy of the temperature control is therefore important for the reproducibility of the productivity, especially at the lowest temperature. The model-form uncertainty is characterized by the leave-one-out errors (Table 4). The measurement uncertainty must be added using the instrument accuracies (Section 2.1); for illustration, relative uncertainties of 2% in both energy and productivity (assumed values, not measured ones) would give u(SEC)/SEC ≈ 2.8%.

Table 7. Change in the model outputs (%) for a set-point change of ±2 °C in temperature (*) and of +0.05 atm in pressure (**). * The pressure follows the saturation line (constant $P/P_s(T)$); the perturbed points lie inside the calibrated corridor. ** At constant temperature; extrapolation inside the admissible domain (P/P_s = 1.09–1.19), qualitative only. n/a: the perturbed point lies outside the admissible domain (75–100 °C, $P_s(T) \le P \le 1$ atm).

Change	Output	75 °C/0.4 atm	85 °C/0.6 atm	90 °C/0.7 atm	100 °C/1 atm
T − 2 °C *	Productivity	n/a	−8.0	−6.2	−1.8
	Total energy	n/a	−5.3	−5.0	−4.5
	SEC	n/a	+2.9	+1.3	−2.8
T + 2 °C *	Productivity	+13.0	+7.8	+5.7	n/a
	Total energy	+5.9	+5.5	+5.2	n/a
	SEC	−6.3	−2.1	−0.5	n/a
P + 0.05 atm **	Productivity	−21.5	−14.6	−12.7	n/a
	Total energy	−3.6	−1.3	−0.8	n/a
	SEC	+22.7	+15.6	+13.6	n/a

4.2. Economic Aspects and Comparison with the Literature

The cost of the distillate was not calculated in this study, because the input data required by the cost models reported for desalination are not available for a bench unit. In these models [43–45], the total annualized cost is the sum of the annualized capital cost and the annual operating cost. The capital cost follows from equipment-cost correlations that are power functions of the heat-transfer areas of the evaporator and the condenser, and the labor and chemical costs are expressed as specific costs per cubic meter of water; for example, EUR 0.02/m³ of freshwater for labor [43,44] and EUR 0.015/m³ of treated feed water for chemicals [43]. A fixed annual labor allowance for a bench unit is not consistent with these specific costs, because, at a productivity of 0.125–0.334 kg/h, it would be spread over less than 3 m³ of water per year even in continuous operation.

A cost calculation for the present unit with these models is not meaningful for three reasons. First, the heat-transfer areas of the evaporator and the condenser of the bench unit were not recorded (Section 2.1), so the equipment cost cannot be obtained from the correlations. Second, the correlations and unit costs were applied to units of much larger capacity; for example, the domestic vacuum desalination system of [44] produces about 21 L/h, i.e., roughly 60–170 times more than the present unit (0.125–0.334 kg/h), and small-scale desalination is generally defined by a capacity below 25 m³/day [39]. Third, the bench

unit was heated electrically, whereas the low-temperature vacuum concept is intended for waste or solar heat; the cost of this heat depends on the heat-pump and photovoltaic–thermal subsystem, which was not part of the measured balances (Section 2.1).

The only cost-related quantity that follows directly from the present measurements is the electricity demand. With the measured specific energy consumption of 3.8–5.7 kWh/kg (3800–5700 kWh/m^3) and the electricity prices of EUR 0.052–0.24/kWh used for different locations in [43], electricity alone would cost about EUR 200–1400/m^3 (no currency conversion is applied). This is roughly 10–90 times higher than the USD 15–18/m^3 reported for autonomous solar membrane distillation units [41] and above the range of USD 0.2–22/m^3 reported for small–medium-scale solar desalination plants [40] (Section 1.2). Electric heating, as used in the bench tests, is therefore not compatible with economical operation, and the potential of low-temperature vacuum distillation depends on supplying the heat from waste or solar sources. A cost assessment with the models of Refs. [43–45] should follow a system-level design of the unit, including the heat-pump and photovoltaic–thermal subsystems; this is outside the scope of the present study.

5. Conclusions

A laboratory thermal vacuum distiller for seawater preheated in a hybrid heat pump was investigated experimentally at four regimes (75–100 °C, 0.4–1 atm) and described by a calibrated semi-empirical model. Prospective applications in hot climates and for autonomous sea navigation are not demonstrated by the present data, because the heat pump and the photovoltaic subsystem were not included in the measured balances. The delivery of distilled water to remote areas by unmanned aerial vehicles in postal packages is a prospective application that was not studied. The main results are as follows.

1. A laboratory stand for producing distillate from seawater preheated in a hybrid heat pump has been developed. The 5 L batch distiller produced 125–334 g/h of distillate at 75–100 °C.

2. The energy and exergy balances of the heating and distillation stages were formulated and quantified for the four regimes (Sections 2.2–4).

3. The calibrated model reproduces the measured productivity within 2.7% and the total energy within 4.5%. This characterizes the fit only: in leave-one-out cross-validation the errors reach 94% (productivity) and 30% (total energy), so the predictive capability of the model is limited. The only interpolation test available (the two interior regimes, errors of about 6%) rests on two data points and is not a validation; the model should therefore be regarded as a descriptive fit of the four measured regimes, suitable only for indicating qualitative trends inside the calibrated corridor of 75–100 °C along the saturation line, and it must not be used for extrapolation. The eight parameters are fitted to twelve measured values, and no independent validation data are available.

4. The measured specific energy consumption is 3.8–5.7 Wh/g, with the lowest value of 3.8 Wh/g at 90 °C/0.7 atm, which is practically equal (within 3%) to that at 100 °C/1 atm. A comparison of vacuum and atmospheric distillation at the industrial scale was not performed in this study. The vacuum regime 75 °C/0.4 atm has the highest specific energy consumption (5.68 Wh/g); the measurements therefore do not demonstrate an energy advantage of vacuum over atmospheric operation.

5. The model must be constrained to physically admissible conditions ($\eta_{heat} \geq 1$, $Q_{maint} > 0$, $f_{evap} > 0$ and $P \geq P_s(T)$); on the 50–100 °C and 0.3–1 atm grid, 75% of the points violate at least one of these constraints.

6. The effect of pressure on the productivity cannot be separated from the effect of temperature, because T and P are strongly correlated in the four regimes ($r = 0.993$); the sign of the coefficient c_2 is not statistically established, and experiments at constant temperature with different pressures are required.

https://doi.org/10.3390/en19215379

7. Within the admissible domain, the model gives the lowest specific energy consumption of about 3.77 Wh/g near 93 °C/0.78 atm, only 3% below the measured value at 90 °C/0.7 atm and within the model deviation; the optimum cannot be resolved. The measured data do not support a preference for the 75 °C/0.4 atm regime when the preheating is supplied by solar collectors: even if the heating energy is excluded, the consumption for maintenance alone is 3.2 Wh/g at 75 °C against 2.2–2.4 Wh/g at 85–100 °C.

8. The exergy efficiency of the laboratory vacuum distillation unit is extremely low (1.6–3.2%), with 96.9–98.4% of the fuel exergy not converted into product: 93.8–95.8% is destroyed by irreversibilities and 2.6–3.1% is lost with the residual hot water. The heating stage accounts for 41–44% of the exergy destruction and the evaporation–condensation–vacuum stage for 56–59%; a split by individual components requires separate metering. On the minimum-work basis, the second-law efficiency is only 0.014–0.020%.

9. The lowest specific energy consumption among the four regimes is 3.875 Wh/g at 90 °C/0.7 atm; its difference from 100 °C/1 atm (3.990 Wh/g) is smaller than the model deviation.

Recommendations for improving efficiency include the following: (1) improving the thermal insulation of the evaporator to reduce exergy destruction; (2) recovering the heat from condensation to preheat the feed water; (3) scaling up the installation and operating it with waste or solar heat; (4) achieving system-level balance, including the hybrid heat pump and the photovoltaic–thermal panel, which is required to quantify the benefit of renewable energy; (5) performing independent validation of the model at intermediate regimes, for example at 80 and 95 °C, and at constant temperature with different pressures; and (6) separate metering of the heater, vacuum pump and condenser together with a specification of the instrument uncertainties.

Author Contributions: Conceptualization, E.V.S., K.V.O. and A.S.M.; data curation, E.V.S. and K.V.O.; formal analysis, E.V.S., K.V.O. and N.A.P.; investigation, E.V.S. and K.V.O.; methodology, E.V.S., K.V.O. and A.S.M.; project administration, K.V.O.; supervision, E.V.S. and K.V.O.; validation, A.S.M. and N.A.P.; visualization, K.V.O.; writing—original draft, K.V.O. and N.A.P.; writing—review and editing, E.V.S., K.V.O. and N.A.P. All authors have read and agreed to the published version of the manuscript.

Funding: The study was supported by the Russian Science Foundation grant No. 25-19-20060, https://rscf.ru/en/project/25-19-20060/ (accessed on 12 September 2026).

Data Availability Statement: Data are available upon request to the corresponding author.

Conflicts of Interest: The authors declare no conflicts of interest.

References

1. Xiao, Y.; Yuan, H.; Shen, J.; Yan, S. Simulation Analysis of Double-effect Seawater Desalination System Using Compression Heat Pump. *J. Phys. Conf. Ser.* **2022**, *2329*, 012013. https://doi.org/10.1088/1742-6596/2329/1/012013.
2. Ghiasirad, H.; Gholizadeh, T.; Javanfam, F.; Rostamzadeh, H.; Skorek-Osikowska, A. Indirect integration of a thermal-mechanical heat pump with a humidification-dehumidification desalination unit. *Appl. Therm. Eng.* **2023**, *230*, 120852. https://doi.org/10.1016/j.applthermaleng.2023.120852.
3. Wang, L.; Zheng, H.; Zhao, Y.; Ma, X. Solar-driven natural vacuum desalination system with inner condenser. *Appl. Therm. Eng.* **2021**, *196*, 117320. https://doi.org/10.1016/j.applthermaleng.2021.117320.
4. Mendonca, S.; Barmavatu, P.; Deshmukh, S.A. Optimizing solar desalination efficiency through vacuum-assisted heat exchanger technology. *J. Therm. Anal. Calorim.* **2025**, *150*, 21047–21066. https://doi.org/10.1007/s10973-025-15061-3.
5. Wang, B.; Shen, J.; Jiang, L.; Wei, W. Research on Two-stage Humidification-dehumidification Heat Pump Desalination System. *J. Phys. Conf. Ser.* **2023**, *2473*, 012003. https://doi.org/10.1088/1742-6596/2473/1/012003.
6. Khalifa, A.; Mezghani, A.; Alawami, H. Analysis of integrated membrane distillation-heat pump system for water desalination. *Desalination* **2021**, *510*, 115087. https://doi.org/10.1016/j.desal.2021.115087.

7. Takalkar, G.; Bhosale, R. Mathematical modeling, simulation and optimization of solar thermal powered Encontech engine for desalination. *Sol. Energy* **2018**, *172*, 104–115. https://doi.org/10.1016/j.solener.2018.07.081.
8. Idrees, H.; Ali, S.; Sajid, M.; Rashid, M.; Khawaja, F.I.; Ali, Z.; Anwar, M.N. Techno-Economic Analysis of Vacuum Membrane Distillation for Seawater Desalination. *Membranes* **2023**, *13*, 339. https://doi.org/10.3390/membranes13030339.
9. Rosyad, M.S.; Ramadhani, S.; Riski, I.; Sutanto, H.S.; Wahyono, Y.; Indrawan, W. Seawater distillation using vacuum pumps and ultraviolet lights to improve desalination process and freshwater quality. *IOP Conf. Ser. Mater. Sci. Eng.* **2020**, *850*, 012008. https://doi.org/10.1088/1757-899X/850/1/012008.
10. Amin, Z.M.; Hawlader, M.N.A. Analysis of solar desalination system using heat pump. *Renew. Energy* **2015**, *74*, 116–123. https://doi.org/10.1016/j.renene.2014.07.028.
11. Rashid, A.; Ayhan, T.; Abbas, A. Natural vacuum distillation for seawater desalination—A review. *Desalin. Water Treat.* **2016**, *57*, 26943–26953. https://doi.org/10.1080/19443994.2016.1172264.
12. Thu, K.; Saha, B.B.; Chakraborty, A.; Chun, W.G.; Ng, K.C. Study on an advanced adsorption desalination cycle with evaporator-condenser heat recovery circuit. *Int. J. Heat Mass Transf.* **2011**, *54*, 43–51. https://doi.org/10.1016/j.ijheatmasstransfer.2010.09.065.
13. Perekopnaya, Y.A.; Osintsev, K.V.; Toropov, E.V. Principles of energy conversion in thermal transformer based on renewable energy sources. In *Advances in Automation. RusAutoCon 2019*; Radionov, A., Karandaev, A., Eds.; Lecture Notes in Electrical Engineering; Springer: Cham, Switzerland, 2020; Volume 641. https://doi.org/10.1007/978-3-030-39225-3_45.
14. Osintsev, K.; Aliukov, S. ORC technology based on advanced Li-Br absorption refrigerator with solar collectors and a contact heat exchanger for greenhouse gas capture. *Sustainability* **2022**, *14*, 5520. https://doi.org/10.3390/su14095520.
15. Shishkov, A.N.; Osintsev, K.V. Modernization of technological equipment in the waste water purification process behind the coke oven using the organic Rankine cycle. In *IOP Conference Series: Materials Science and Engineering, Volume 1064, International Conference on Mechanical Engineering, Automation and Control Systems (MEACS 2020) 17 September 2020, Novosibirsk, Russian Federation*; IOP Publishing Ltd.: Bristol, UK, 2021; Volume 1064, p. 012032. https://doi.org/10.1088/1757-899X/1064/1/012032.
16. Mirmanto, M.; Mulyanto, A.; Lestari, D.D. Effect of the number of turns of a coil evaporator on water production. *IOSR J. Mech. Civ. Eng.* **2022**, *19*, 31–35 https://doi.org/10.9790/1684-1904023135.
17. Tsatsaronis, G. Thermoeconomic analysis and optimization of energy systems. *Prog. Energy Combust. Sci.* **1993**, *19*, 227–257.
18. Bejan, A.; Tsatsaronis, G.; Moran, M. *Thermal Design and Optimization*; Wiley: New York, NY, USA, 1996.
19. Kotas, T.J. *The Exergy Method of Thermal Plant Analysis*; Butterworths: London, UK, 1985.
20. Mirmanto Mirmanto, N. Nurchayati Performance of Air-Water Harvester Machine for Cooling Drinking Water. 2022. https://doi.org/10.9790/1684-1902020106..
21. Mirmanto, M.; Syahrul, S.; Wijayanta, A.T.; Mulyanto, A.; Winata, L.A. Effect of evaporator numbers on water production of a free convection air-water harvester. *Case Stud. Therm. Eng.* **2021**, *27*, 101253. https://doi.org/10.1016/j.csite.2021.101253.
22. Siricharoenpanich, A.; Wiriyasart, S.; Prurapark, R.; Naphon, P. Effect of cooling water loop on the thermal performance of air conditioning system. *Case Stud. Therm. Eng.* **2019**, *15*, 100518. https://doi.org/10.1016/j.csite.2019.100518.
23. Wu, X.P.; Johnson, P.; Akbarzadeh, A. Application of heat pipe heat exchangers to humidity control in air conditioning systems. *Appl. Therm. Eng.* **1997**, *17*, 561–568.
24. Khedari, L.; Permchart, W.; Pratinthong, N.; Hirunlabh, J. Field study using the ground as heat sink for the condensing unit of an air conditioner in Thailand. *Energy* **2001**, *26*, 797–810.
25. Martinez, F.J.R. Design and experimental study of a mixed energy recovery system, heat, heat pipes and indirect evaporative equipment for air conditioning system. *Energy Build.* **2003**, *35*, 1021–1030.
26. Yau, Y.H. Experimental thermal performance study of an inclined heat pipe heat exchanger operating in high humid tropical HVAC systems. *Int. J. Refrig.* **2007**, *30*, 1143–1152.
27. Yau, Y.H. Application of a heat pipe heat exchanger to dehumidification enhancement in tropical HVAC systems-a baseline performance characteristics study. *Int. J. Therm. Sci.* **2007**, *46*, 164–171.
28. Yau, Y.H. The use of a double heat pipe heat exchanger system for reducing energy consumption of treating ventilation air in an operating theatre—A full year energy consumption model simulation. *Energy Build.* **2008**, *40*, 917–925.
29. Wan, J.W.; Zhang, J.L.; Zhang, W.M. The effect of heat-pipe air-handling coil on energy consumption in central air-conditioning system. *Energy Build.* **2007**, *39*, 1035–1040.
30. El-Baky, M.A.; Mohamed, M.M. Heat pipe heat exchanger for heat recovery in air conditioning. *Appl. Therm. Eng.* **2007**, *27*, 795–801.
31. Alklaibi, A.M. Evaluating the possible configurations of incorporating the loop heat pipe into the air-conditioning systems. *Int. J. Refrig.* **2008**, *31*, 807–815.

32. Naphon, P. On the performance of air conditioner with heat pipe for cooling air in the condenser. *Energy Convers. Manag.* **2010**, *51*, 2362–2366.
33. Mirmanto, M.; Wirawan, M.; Sayoga, I.M.A.; Syahrul, S.; Faisal, M.; Abdullah, A. Effect of absorber types of conventional distillers on the amount of distilled water production. *Front. Heat Mass Trans.* **2019**, *13*, 1–7. https://doi.org/10.5098/hmt.13.10.
34. Gugulothu, R.; Somanchi, N.S.; Reddy, K.V.K.; Gantha, D. A review on solar water distillation using sensible and latent heat. *Procedia Earth Planet. Sci.* **2015**, *11*, 354–360. https://doi.org/10.1016/j.proeps.2015.06.072.
35. Panchal, H.; Patel, P.; Patel, N.; Thakkar, H. Performance analysis of solar still with different energy absorbing materials. *Int. J. Ambient Energy* **2015**, *38*, 224–228. https://doi.org/10.1080/01430750.2015.1086683.
36. He, W.; Yang, H.; Han, D. Thermodynamic investigation and optimization of a heat pump coupled open-air, open-water humidification dehumidification desalination system with a direct contact dehumidifier. *Desalination* **2019**, *469*, 114101. https://doi.org/10.1016/j.desal.2019.114101.
37. Sharan, P.; McTigue, J.; Yoon, T.J.; Currier, R.; Findikoglu, A. Energy efficient supercritical water desalination using a high-temperature heat pump: A zero liquid discharge desalination. *Desalination* **2021**, *506*, 115020. https://doi.org/10.1016/j.desal.2021.115020.
38. Glushenkov, M.; Bhosale, R.; Kumar, A.; Almomani, F.; Kronberg, A. Heat Powered Water Pump for Reverse Osmosis Desalination. In *Materials for Energy, Efficiency and Sustainability*; CRC Press: Boca Raton, FL, USA, 2016; pp. 201–204, ISBN 978-0-9975-1171-0.
39. Kariman, H.; Shafieian, A.; Khiadani, M. Small scale desalination technologies: A comprehensive review. *Desalination* **2023**, *567*, 116985.
40. Zhang, Y.; Sivakumar, M.; Yang, S.; Enever, K.; Ramezanianpour, M. Application of solar energy in water treatment processes: A review. *Desalination* **2018**, *428*, 116–145.
41. Banat, F.; Jwaied, N. Economic evaluation of desalination by small-scale autonomous solar-powered membrane distillation units. *Desalination* **2008**, *220*, 566–573.
42. Poling, B.E.; Prausnitz, J.M.; O'Connell, J.P. *The Properties of Gases and Liquids*, 5th ed.; McGraw-Hill: New York, NY, USA, 2001.
43. Filippini, G.; Al-Obaidi, M.A.; Manenti, F.; Mujtaba, I.M. Design and economic evaluation of solar-powered hybrid multi effect and reverse osmosis system for seawater desalination. *Desalination* **2019**, *465*, 114–125. https://doi.org/10.1016/j.desal.2019.04.016.
44. Kariman, H.; Hoseinzadeh, S.; Shirkhani, A.; Heyns, P.S.; Wannenburg, J. Energy and economic analysis of evaporative vacuum easy desalination system with brine tank. *J. Therm. Anal. Calorim.* **2020**, *140*, 1935–1944. https://doi.org/10.1007/s10973-019-08945-8.
45. Al-Obaidi, M.A.; Filippini, G.; Manenti, F.; Mujtaba, I.M. Cost evaluation and optimisation of hybrid multi effect distillation and reverse osmosis system for seawater desalination. *Desalination* **2019**, *456*, 136–149.

Disclaimer/Publisher's Note: The statements, opinions and data contained in all publications are solely those of the individual author(s) and contributor(s) and not of MDPI and/or the editor(s). MDPI and/or the editor(s) disclaim responsibility for any injury to people or property resulting from any ideas, methods, instructions or products referred to in the content.